

Structures Produced by the Collision of Extragalactic Jets with Dense Clouds

S.W. Higgins^{1,3}, T.J. O’Brien¹ & J.S. Dunlop²

¹ *Astrophysics Research Institute, Twelve Quays House, Egerton Wharf, Birkenhead L41 1LD, UK*

² *Institute for Astronomy, University of Edinburgh, Blackford Hill, Edinburgh, EH9 3HJ, UK*

³ *Current address: Dept. Computing and Mathematics, Manchester Metropolitan University, John Dalton Building, Chester Street, Manchester, UK*

e-mail: S.Higgins@doc.mmu.ac.uk, tob@astro.livjm.ac.uk, jsd@roe.ac.uk

6 November 2018

ABSTRACT

We have investigated how several parameters can affect the results of a collision between an extragalactic jet and a dense, intergalactic cloud, through a series of hydrodynamic simulations. Such collisions are often suggested to explain the distorted structures of some radio jets. However, theoretical studies of this mechanism are in conflict over whether it can actually reproduce the observations.

The parameters are the Mach number, and the relative densities of the jet and the cloud to the ambient medium. Using a simple prescription we have produced synthetic radio images for comparison with observations. These show that a variety of structures may be produced from simple jet-cloud collisions. We illustrate this with a few examples, and examine the details in one case. In most cases we do not see a clear, sustained deflection. Lighter jets are completely disrupted. The most powerful jets produce a hotspot at the impact which outshines any jet emission and erode the cloud too quickly to develop a deflected arm. It appears that moderate Mach numbers and density contrasts are needed to produce bends in the radio structure. This explains the apparent conflict between theoretical studies, as conclusions were based on different values of these parameters. Shocks are produced in the ambient medium that might plausibly reproduce the observed alignment of the extended emission line regions with the radio axis.

Key words: galaxies: active, galaxies: jets, hydrodynamics, shock waves

1 THE EFFECT OF ENVIRONMENT ON EXTRAGALACTIC JETS

1.1 Complex and distorted structure in extragalactic radio sources

The jets and hotspots of radio galaxies and quasars often show complex structure, including bends, twists, knots and multiple hotspots. Such structure is seen over a huge range of sizes, from the enormous wide-angle tail (WAT) sources (which can be megaparsecs in size), to the compact steep-spectrum (CSS) sources (which are about 10–15 kpc across). Jets can appear to bend by over 90° and remain collimated for several jet radii (Bridle & Perley 1984), despite the expectation that the oblique shock causing the bend should decelerate the jet. Explanations for these complex structures include motion through some intra-cluster medium (Leahy 1984), perturbations due to mergers (van Breugel et al. 1986, Sakelliou, Merrifield & McHardy 1996), variations in the direction of the jet at its source (Williams & Gull 1985,

Scheuer 1982), and collision with dense clouds in the ambient medium (Burns 1986). Cloud collisions are particularly applicable in cases where these bends are very sharp. Other models would produce more gradual bends.

Theoretical studies of jet-cloud collisions appear to be in conflict over whether they can explain the observations. In some previous numerical simulations the jet is decelerated and effectively disrupted by the cloud, and the cloud is subsequently destroyed (De Young 1991). In others the jet appears to remain collimated as it is re-accelerated in a new direction (Norman 1993). Most recently Raga & Canto (1996) find from two-dimensional simulations and analytical studies that the jet bores through the cloud but reaches a steady configuration. In this paper we describe the results of a study aimed at resolving this question by investigating the effects of various hydrodynamical and geometrical parameters. This investigation uses three-dimensional, adiabatic simulations. We also follow the development of the interactions for a longer time than previous simulations, and estimate the in-

tensity of synchrotron emission from the jet to enable meaningful comparison with observed radio maps.

Through these studies we hope to be able to determine what types of complex structure can be explained by jet-cloud collisions. Such studies could shed light on the alignment between radio and optical axes in high redshift radio galaxies, the contribution of shocks to the spectra of extended emission lines regions and the role of environmental effects in unified schemes for AGN and their evolution.

1.2 Examples of distorted structure

Wide-angle tail (WAT) sources are found in rich clusters and have distorted, C-shaped structure. Large WATs approaching 1 Mpc across cannot be bent by the motion of the parent galaxy through the cluster without assuming unreasonably high speeds through unreasonably dense intra-cluster gas (Burns 1986). To satisfy the requirements of momentum balance and to reproduce the sharpness of the bends that are observed, Burns proposed that the jets may collide with clouds of higher density in the surrounding medium. A good example is the western jet of the WAT 1919+479, which emerges from the core, vanishes after a short distance, and then reappears at a bright hotspot (Burns et al. 1986, Pinckney et al. 1994). Beyond this hotspot a tail stretches out for 800 kpc in a direction about 90° to that of the original jet, broadening and fading as it does so. The bend here is very sharp. There is one other hotspot not far from the beginning of the tail. Rotation measure and depolarisation are described as ‘patchy’, and vary significantly over the tail. X-ray observations show large scale asymmetry in the intra-cluster medium. The simulations of Loken et al. (1995) show that the necessary gas velocities can arise in cluster mergers, as can shocks that will bend the jet. However, these simulations still do not explain the sharpness of the bend or the persistence of the halo.

Barthel et al. (1988) present a large sample of quasars with powers greater than the Fanaroff-Riley division but distorted structures. Twenty out of a sample of eighty high-redshift quasars showed bending greater than 20° , instead of the classical double structure that would be expected.

Compact Steep Spectrum (CSS) sources make up 10–15% of AGN. More than 15% have axes between the lobes and the core that are misaligned by more than 20° (Saikia et al. 1995). This distortion seems to be associated with an asymmetrical ambient medium.

In quasars the most prominent jets are in complex or one-sided structures, and smaller sources are the more powerful (Muxlow & Garrington 1991). Stocke, Burns and Christiansen (1985) present observations of ‘dogleg’ quasars showing strong changes in direction within the lobes. There is no evidence that these sources are found any more often in rich or poor cluster environments, a conclusion supported by recent work (Rector, Stocke & Ellingson 1995). Only a few dense clouds are needed in each case to explain the proportion of bent jets, so it would appear that it is the inhomogeneity of the environment, not its overall density, that causes the bends.

1.3 Intergalactic clouds in the neighbourhood of extragalactic jets

Evidence for inhomogeneity in the medium surrounding AGN comes from measurements of depolarization and line emission, and correlations between these properties/features and the radio structure.

Maps of rotation measure and depolarization of a sample of radio sources show significant inhomogeneity on a range of scales, some as low as 5kpc, some larger than 50kpc, out to distances of about 100kpc from the nuclei (Pedelty et al. 1989). Such effects could be caused by density inhomogeneities in the surrounding material.

The infrared, optical and ultraviolet structures of many high-redshift radio galaxies are closely aligned with the radio structures (McCarthy 1993, Chambers, Miley & van Breugel 1987). There are also several correlations between line emission and other aspects of distorted jets, for example: brighter line emission occurs on the side of the nearer radio-lobe (McCarthy, van Breugel & Kapahi 1991); the level of blue light and the strength of the alignment effect are correlated with a mix of radio power and spectral index (Dunlop & Peacock 1993). The lobes of these radio sources are often asymmetrical with the lobe nearer the nucleus tending to be more depolarized than the more distant lobe (Liu & Pooley 1991), suggesting that the material responsible for the depolarization may also present more resistance to the jet.

Regions of optical line emission are associated with knots and bends in the jets (Wilson 1993). For example, the radio galaxy 4C 29.30 has a region of line emission close to a bright knot just before a bend (van Breugel et al. 1986). The radio galaxy PKS2250-41 shows extended emission aligned with the radio axes, including a large arc-shaped region of line emission surrounding the radio lobe (Tadhunter et al. 1994). Extended emission line regions have a “clear spatial association” with regions of depolarized radio emission (Baum & Heckman 1989).

In many sources (especially at higher redshifts) the spectra from this extended emission line region can only be explained if a significant shock component is included (Clark & Tadhunter 1996, and references therein). Low polarization of the ultra-violet emission shows that there is not enough scattered AGN emission to account by itself for the total flux (Tadhunter 1996). The cloud collision model is now commonly invoked to explain the properties of extended emission line regions in AGN, for example the Seyfert galaxy NGC 1068 (Axon 1996); radio galaxies 3C 254 (Crawford 1996) and 3C368 (Stockton, Ridgway & Kellog 1996); and Cen A (Sutherland, Bicknell & Dopita 1993), as well as the sources mentioned in the previous paragraph.

The most luminous radio sources are known from observations to reside in regions of high galaxy density (Yates, Miller & Peacock 1989, Hill & Lilly 1990). X-ray observations of powerful radio galaxies and quasars show that many lie in the centres of rich clusters with dense, rapidly cooling IGM in which cold clouds can condense (Fabian 1993). Cowie et al. (1983) observed filamentary line emission in cooling flows that could indicate the presence of such clouds. Observations suggest that these clouds have temperatures of about 10^4 K, densities of about 100 cm^{-3} and sizes of 3–15kpc (Baum 1992). Some contribution from radio jets seems necessary to re-energize the filaments.

2 SIMULATING COLLISIONS OF JETS AND CLOUDS

2.1 Previous simulations

Analytical studies show that sharp bends of 90° are possible if the jet is thin or only moderately supersonic (Icke 1991). More recently Raga & Canto (1996) have published analytical calculations and two-dimensional simulations showing bending by clouds. They conclude that slower jets will be bent more, and clouds will be eroded as jets bore through them.

The first investigation of the effect of off-axis jet-cloud collisions was by De Young (1991) using the ‘beam scheme’ (Sanders & Prendergast 1974), to test the proposal of Burns (1986) that bending in large WATs is the result of collisions with clouds. De Young monitored the jet flow using test particles, and observed that the jet was considerably decelerated by the impact with the cloud. The cloud was destroyed within a few million years, and the jet returned to its original direction. He concluded that the interaction does not last long enough to produce anything like a tail.

However, WAT tails have a wide opening angle and show no strong evidence of supersonic speeds (such as terminal hotspots). It would appear the jet is disrupted at the impact point anyway. The only question is whether the interaction can be maintained long enough to produce tails of the observed length.

A similar interaction was investigated at higher resolution by Balsara & Norman using their RIEMANN code (Norman 1993). They argued from plots of the velocity field that a De Laval nozzle was formed which re-accelerated the jet in a new direction after impact.

We aimed to resolve this conflict through the work described in this paper, and to more thoroughly investigate the effect of different parameters both on the development of the interaction over time, and the structures produced, and by estimating the appearance of the source at radio wavelengths for direct comparison with observations.

2.2 Numerical techniques

The simulations we present in this paper were performed using a hydrodynamic code based on the Godunov method of Falle (1991) in three-dimensional Cartesian coordinates. This technique solves the inviscid Euler equations to second-order accuracy in space and time, with an adiabatic equation of state. In addition to calculating the usual dynamical variables, we also calculate a parameter representing the fraction of density within each cell which was originally jet material. This allows us to follow the evolution of the jet separately from the ambient medium and to calculate synthetic radio maps as described in section 2.4.

Since we can draw a plane of symmetry bisecting the cloud and containing the jet we have only calculated one half of the region around the interaction (figure 1). The boundaries of this domain are treated as free flow except for the symmetry plane and the region where the jet enters the grid. A free flow condition assumes that values on the outer surfaces of each cell are exactly equal to those on the inner surfaces. The symmetry condition is that velocities normal to the surface are reflected. The jet is produced by using an

appropriate boundary condition representing incoming material in the region where the jet enters. Note we have made no assumptions about the position of the central engine with respect to the grid.

The simulations can be rescaled so that they represent structures on parsec or kiloparsec scales, as long as the gas behaves adiabatically. The simplest rescaling is to change sizes and times in proportion, preserving all other variables. For example, if the cell side is 1 kpc, then 1 time unit = 2×10^6 years. We use this scaling as a reference in discussing the simulations below. We can apply these simulations to other cases with different pressures and temperatures. For example, in the case of the fastest jets, the temperature may be a hundred times higher, or for the slow jets a hundred times lower, and we still have velocities in the range accepted for extragalactic jets.

2.3 Testing the hydrodynamic code

We used the code to calculate two one-dimensional test problems. The first was Sod’s shock tube problem (Sod 1978). The code was used to compute plane shocks moving along each of the three axes of the grid (in both forward and reverse directions, as well as at various resolutions). It produced results in good agreement with the analytical solution.

The second test problem was the collision of a one-dimensional shock with a density discontinuity (Nittman, Falle & Gaskell 1982). This problem is clearly appropriate to our investigation as a useful indication of the fidelity of the code in this case. Once again this was run with shocks and discontinuities normal to each of the three axes, moving both forwards and in reverse directions and at various resolutions. Figure 2 shows an example of the results (full details are given in the caption to the figure). The positions and values of the two shocks were accurately reproduced.

As a final test we re-calculated a portion of one of the simulations (simulation 3 – see section 3.2) at double the initial resolution within a volume one-eighth of the size and compared the results. When the high-resolution results were smoothed to the lower resolution they showed no significant differences. Nor did there appear to be any effects caused by allowing the simulated flow to leave this grid compared to the same region of the lower resolution simulation. In figure 3 we show density slices at the same time for the simulations at both resolutions. We are satisfied from this that the results of our simulations are not significantly affected by the resolution or boundary effects.

2.4 Producing synthetic radio maps

Previous studies of jet-cloud collisions relied on the interpretation of flow patterns produced by the simulations to reach their conclusions. To allow a more direct comparison we have developed a simple approximation for the intensity of synchrotron emission in terms of the hydrodynamic variables. We use this to produce estimates of the surface brightness distribution of radio emission. These synthetic radio maps can be compared with observations. In this section we describe our prescription, and the assumptions it is based on. We then consider how changing these assump-

tions might affect the results, and present some plots for alternative prescriptions.

The intensity j of synchrotron emission at frequency ν is given by $j \propto KB^{1+\alpha}\nu^{-\alpha}$, where B is the magnetic field strength, α is the spectral index and K is related to the number density $N(\gamma)$ of relativistic electrons with Lorentz factors in the range $(\gamma, \gamma + d\gamma)$ via $N(\gamma)d\gamma = K\gamma^{-(2\alpha+1)}d\gamma$. In order to calculate j we need to express the magnetic field and the coefficient K in terms of the results of our hydrodynamic simulations.

To determine the magnetic field we assume that the field is insignificant outside the jet (see, for instance, Smith et al. 1985) and the magnetic flux is frozen into the jet material. By conservation of magnetic flux we would expect the field strength to be related to the jet density via $B \propto \rho_{jet}^{2/3}$. In practise a complicated flow can amplify an initially disordered field. For the purposes of this work we have neglected this amplification.

To determine the coefficient K we assume that the energy density of relativistic particles is a fixed fraction of the internal energy density of the gas with the only changes in the distribution being due to adiabatic expansion. This is equivalent to assuming that the relativistic electrons form a supra-thermal tail throughout the gas, and the efficiency of the acceleration process is similar everywhere. Following Wilson and Scheuer (1983) we can relate K to the gas pressure p via $K \propto p^{(\alpha/2+3/4)}$. The adiabatic index varies between $5/3$ for non-relativistic gas to $4/3$ for relativistic particles which corresponds to an uncertainty of about 0.3 in our choice of α .

We substitute for K and B from the formulae above, and therefore obtain

$$j\nu^\alpha \propto p^{\alpha/2+3/4} \rho_{jet}^{2\alpha/3+2/3} \quad (1)$$

With $\alpha=0.5$ we have $j\nu^\alpha \propto p\rho_{jet}$, whereas with $\alpha = 1.0$ we find $j\nu^\alpha \propto p^{5/4} \rho_{jet}^{4/3}$.

As an alternative to assuming that magnetic flux is frozen into the jet and that it is zero elsewhere we could assume that the magnetic energy density is in equipartition with the internal energy density of the gas (and, because of our other assumption, with the relativistic particle energy density). This leads to $B \propto p^{1/2}$ and therefore

$$j\nu^\alpha \propto p^{\alpha+5/4} \quad (2)$$

It is common to use $\alpha=0.75$ so that $j\nu^\alpha \propto p^2$.

Further, if one still believed that the magnetic field was negligible outside the jet then we could use this expression with one's favourite α wherever $\rho_{jet} \neq 0$ and set the intensity equal to zero where $\rho_{jet} = 0$.

We can calculate the synchrotron intensity for each computational cell and, assuming that the emission is optically thin, integrate along lines of sight to produce a synthetic radio map at any epoch. In figure 4 (a – d) we show four alternative maps from the same fluid conditions based on the alternatives described above (see caption). Using the square of total pressure, the hotspot is large with a shape like a tadpole, but neither the jet nor the deflected tail are detectable. However, the evidence for higher magnetic fields in the jet is strong. The other alternatives produce structures that are similar to each other, so that the general comparisons we would like to make are not seriously affected.

3 THE EFFECT OF JET AND CLOUD PROPERTIES ON THE RESULTS OF THE INTERACTION

3.1 Models and coverage of parameter space

The parameter space of jet cloud collisions is multi-dimensional. In an attempt to explore the range of behaviour within this space we have chosen to vary the values of three of the most significant parameters over ranges applicable to extragalactic jets: the jet Mach number, its density contrast with the ambient medium, and the contrast between cloud and ambient density. Using one of these cases, we have also investigated the effect of impact angle and relative size of cloud and jet on one of the more interesting cases. Details are given in table 1.

We have assumed conditions in the ambient medium consistent with observations, that is a temperature of $5 \times 10^7 \text{K}$ and a particle number density of 0.01cm^{-3} . These values are used to normalize the quantities in the computation so that model values for the ambient density and pressure in the code are set to 1.0. The jet and cloud are both taken to be in pressure balance with the ambient medium. The computational domain is divided into a grid of $50 \times 120 \times 120$ cells.

3.2 Summary of results

By simply changing a few parameters we have produced a range of different structures. We discuss these in this section. The common features in all the simulations are: the jet is disrupted and decelerated to some extent on collision; the cloud is eroded by the jet; high pressures and densities are produced at the point of impact, giving rise to bright hotspots in the radio emission. All these structures vary in time, and many might be associated with features observed in real radio sources at different epochs in the simulation (Higgins, O'Brien, & Dunlop, 1995).

We illustrate this discussion by presenting some examples. In each case we show total density beside a synthetic radio map at two epochs. Density plots show a slice through the symmetry plane (see figure 1), rendered in a logarithmic greyscale. The synthetic radio maps are produced by estimating the intensity of synchrotron emission in each cell (using the formula $j\nu^\alpha \propto p\rho_{jet}$, as described in section 2.4). This is then summed along the line-of-sight perpendicular to the symmetry plane. The resulting maps are shown on a logarithmic greyscale with a range of about one order of magnitude. They have very different peak values, so the hotspots are not directly comparable, but the dynamic range between the peaks and faintest features are. The faster jets have left the grid in all cases before the slower jets have developed any interesting features, so we show each jet shortly after impact, and then at a later stage of the interaction. For the fast jet this is $t=4$ units of computational time after it enters the grid (16 million years on the scaling specified above) and $t=28$ (56 million years). The slower jets are also shown at $t=28$, which is around the time of impact, and then at $t=76$ (112 million years).

The light, slow jet (simulation 1, figure 5) is scattered into a very broad area in all directions perpendicular to the jet. A mushroom or umbrella shaped structure is formed in

the radio emission. The hotspot is no brighter than it was in the ambient medium before impact, and is recessed a little within the lobe. It is not obvious from the radio structure that this is a cloud collision. When the same jet encounters a denser cloud (simulation 2) the interaction lasts longer, since the jet erodes the cloud much more slowly. The denser cloud makes no difference to the hotspot behaviour, which is not significantly brighter on impact with the cloud. This feature almost certainly depends on the relative sizes of the jet and cloud: a much larger cloud would not allow deflection in both directions.

The fast, light jet (simulations 3 and 4, figure 6) produces a weak secondary hotspot at the head of the deflected jet in the radio map. This is about a tenth as bright as the spot at the impact point. It becomes disconnected (on the dynamic range of our radio plots) and disappears within about fifty thousand years, and the jet rapidly erodes the cloud (whatever its density). As the jet breaks through the cloud there are two hotspots within a boot-shaped lobe. Although the cloud impact is the cause of the bending, the deflection and secondary hotspot is actually produced as the jet bends inside the distorted cocoon that has been formed during the interaction.

After a few hundred thousand years it has broken through the cloud and shot off the grid. This faster jet can be deflected, and produces much more visible results, but only for a short time. In this case the hotspot shows a small increase in brightness (about 10 – 20%) on impact, and remains about the same throughout the interaction. The density of the cloud does not make significant difference to the effect on the jet in either of these cases.

The slow, heavy jet (simulations 5 and 6, figure 7) shows a clear deflection by 90° . The jet forms a bowl-shaped cavity in the cloud which deflects the jet with a relatively large radius of curvature. We do not see any secondary hotspot in the radio map. The primary hotspot brightens steadily after impact, up to a factor between two and three. The jet erodes the cloud slowly. On the scale of a WAT source it takes about 3×10^8 years to erode the less dense cloud. There is a hotspot down the jet before the impact point. When the cloud is denser the interaction does of course last longer. The deflection angle is nearer to 70° . After about 6×10^8 years the deflected arm is about four jet radii long, and about half as wide again as the incoming jet. The jet has worked about half way through the cloud. The shape of the deflecting face formed by the interaction is now deeper, so disrupting the jet more. However the interaction can certainly continue for some time yet.

The fast, heavy jet (simulations 7 and 8) pushes deep into the cloud, however dense it may be. The impact hotspot is orders of magnitude brighter than any other features. The jet breaks through the cloud within about 50 million years. The radio map shows an extremely bright deflection spot and weaker secondary (by 1000 times) in the deflected material. The primary hotspot brightens by a factor of ten on impact in this powerful jet. Because this interaction is short-lived, and the hotspot far outshines any other emission, it would be difficult to detect any deflection in a source with this powerful a jet.

3.3 The Effect of Impact Angle

We used the same fluid parameters as in simulation 4, altering only the angle at which the jet encountered the cloud. With an impact angle of 45° this produces a distinct secondary at the head about one jet radius away. However, it is shorter lived (~ 40 million years) and the angle of deflection decreases quickly as the jet erodes the cloud. With an impact angle of 30° the deflection is shallower ($\sim 70^\circ$) and shorter lived. Shallower impact angles can produce secondary hotspots since less momentum is lost by the jet, but the interaction is short lived on the whole. An impact angle of 45° is probably the lower limit for a deflection of 90° .

3.4 An Example of a Jet-Cloud Interaction

Our sixth simulation ($M=2$, $\eta=0.2$, figure 7) shows all the major features of WAT jets: bent sharply through 90° at bright hotspots and flaring out into long, wide tails (O'Donoghue, Eilek & Owen 1990). Due to the higher cloud density the interaction is long-lived. It lasts for something of the order of 10^8 years, which allows the formation of a tail not only large enough but of an age consistent with estimates of travel time to the end of the tails from synchrotron spectral-aging (O'Donoghue, Owen & Eilek 1993).

We chose this simulation to examine the dynamics of the interaction in more detail. In particular we look at the distribution of material and its velocity in three dimensions, along with the estimated radio emission, and how it varies with viewing angle. We also give some indications of the likely location and shape of line emission.

Figure 8 shows velocity vectors plotted in three dimensions, with the initial jet direction emerging from the plane of the diagram. This is at a later time than shown in figure 7 (3×10^8 years). These show how the material is deflected after impact into a fan of opening angle between $60^\circ - 80^\circ$. None of this material is moving slower than 20% of the speed of the incoming jet. A spine of slightly faster material can be discerned along the middle of this fan, representing the remnant of the jet. The wings are material deflected at higher speed on impact; as the interaction progresses the impact cavity deepens and material deflected in this direction at later times has slightly lower speeds that fall below the threshold of this plot. Clearly on deflection the jet is not only decelerated but almost all collimation is lost. However, this fan is very flat, allowing the appearance of a deflected tail when viewed from the side.

The next plots (figure 9) show the expected radio emission, viewed from two orientations. Since the fan is fairly thin this gives a reasonable impression of a bent jet from the side (a), with the tail showing many similarities to WATs, including filamentary structure. This seems to be due to vortex action in the tail. In (b) we see how this radio structure would appear were it not close to the plane of the sky. The emission from the deflected fan now surrounds the whole jet. This emission should not be as bright as the previous case since that had longer path lengths through the emitting material. Thus it should be more difficult to identify the counterparts of these objects at different orientations.

3.5 Line emission

The compression and distortion of the cloud would be likely to result in enhanced line emission, due to photoionization by continuum from a hidden quasar (if not limited by the flux from the nucleus) or shock heating. The simulations show elongated density enhancements beside the jet, especially the transmitted shock driven into the cloud. As a crude indicator of the expected position and distribution of line emission, we have plotted the distribution of density squared (emission measure) integrated through the grid in figure 10. This is overlaid in the figure with contours of radio emission. Note the bright, elongated region inside the cloud, forming a cap around the impact point. Compact regions of line emission are seen in HST images (for example 4C41.17, van Breugel 1996) which we interpret in this model as shock fronts moving away from the jet, providing density enhancements for scattering of or photo-ionization by the AGN continuum, or shock-ionization. This gives a natural explanation for the radio-optical alignment effect.

3.6 The Effect of Several clouds

In realistic situations there are likely to be many clouds, so we have simulated the passage of a jet through a medium containing an ensemble of clouds. Figure 11 shows a three-dimensional rendering of total density and a synthetic radio map at the same epoch. As the jet progresses through the grid it collides with clouds, producing prominent hotspots in the radio emission. These spots persist as the jet moves past the cloud and encounters further obstructions. They fade as the clouds are eroded by the passage of the jet. Meanwhile new hotspots form at new encounters, and deflected jet material percolates through the ambient medium, producing filamentary and foamy shock structures. The result is a jet that is made visible by a series of irregular knots, with a crooked ridgeline, filamentary diffuse bridges and lobes and multiple hotspots at the head of the jet. It clearly remains collimated and produces a bow-shock at its head.

4 CONDITIONS FOR THE DEFLECTION OF JETS

Synchrotron emission may not trace the fluid flow in an extragalactic jet in a simple way. Bends in the radio structure may not represent bends in the flow. Our synthetic radio maps allow us to make more general comparisons between our simulations and observations. De Young and Balsara and Norman based their conclusions solely on the flow patterns. Our results show how a few changes in parameter values can alter the results of a collision. Under our assumptions, it is possible to produce structures reminiscent of those seen in a variety of radio sources. This also explains the apparent conflict between previous simulations. The simulations performed by De Young involved a fast, heavy jet (about Mach 25, with a density contrast of $\eta=1$) so it is not surprising that it ripped up the clouds. In contrast, Balsara and Norman's jet was of a moderate speed and lightness (Mach 4 and a density contrast of $\eta=0.2$). As we have shown it is easier to produce deflection under these conditions. The conclusions clearly depend on the choice of parameter values.

The impact causes a large increase in radio luminosity of fast jets, which can still be seen after tens of millions of years. Samples of ultra-luminous radio sources may contain a large proportion of sources in which jets have been in collision with clouds within this time in their past, even if the probability of a collision is fairly small for any source. The technique of ultra-steep-spectrum selection used to locate luminous sources at high redshift (Rottgering 1992) could make this bias even stronger.

The range of structures we have produced suggest that deflection may be easier to produce or detect in lower power jets propagating in the plane of the sky. We attempt to model sources in more detail in future papers, but note that in the case of WATs these do not seem very demanding requirements: the sizes are already very large, so we would not expect any other orientation. When such sources are seen at some other orientation the lobe emission may be too diffuse to detect. However, our simulations use spherical clouds, which are clearly an idealised case. Other shapes or clouds with some density variation may produce a better degree of collimation in the deflected jet. This might allow deflected structures to be observed from a wider range of angles. Larger clouds may sustain the deflection of high power jets long enough to produce a deflected arm.

Steffen et al. 1997 have studied the interaction of jets with clouds in the narrow-line region of Seyfert galaxies through two-dimensional, non-adiabatic simulations. These suggest that only clouds above a critical density will radiate after being shocked by the impact of the jet. Thus the absence of detectable emission associated with bends may be due to a low cloud density.

We have also tentatively associated our other simulations with bent structure. We discuss this in detail elsewhere. In particular we find that different structures may be produced by a single set of parameters as the interaction progresses (Higgins, O'Brien & Dunlop 1995, Dunlop 1995). Other sources can also be modelled by these simulations (with rescaling when appropriate). Our studies show that shallower impact angles can produce secondary hotspots since less momentum is lost by the jet, although these are short-lived. Thus compact sources seem to be best modelled with more oblique impacts and/or several clouds (see figure 6).

4.1 Further Development

In conclusion, given the right sets of conditions collisions between jets and clouds can reproduce some of the distorted structure seen in observations, and is suggestive of alignments between radio and optical axes. A more detailed understanding of the physics involved could allow us to infer the properties of jets and their environment.

The radio maps presented here assume a fixed spectral index throughout the source. A more sophisticated prescription in which this could vary would allow us to investigate the variation of the appearance of a source with frequency. It should also be possible to include calculation of a few common lines, and their spatial distribution.

These calculations are non-relativistic. Relativistic simulations of jets show no gross differences to the structures seen in non-relativistic simulations. The most significant difference is in the effect of Doppler beaming, which should not

apply in our case since the lobes are not beamed. Recent calculations suggest that relativistic jets may lose less kinetic energy through entrainment of ambient material (Bowman, Komissarov & Leahy 1996). If this was the case in our model it might allow better collimation after deflection. We intend to make relativistic calculations to explore this possibility.

ACKNOWLEDGMENTS

SWH acknowledges the PPARC for receipt of a studentship, and his wife, Leah, and parents for additional financial subsidies. Computing was performed using the Liverpool John Moores University Starlink node. We would like to thank Dr Sam Falle for useful suggestions, and Dr Huw Lloyd and Dr John Porter for valuable discussions and the referee for pointing out important considerations.

REFERENCES

- Axon, D., 1996, in Clark, N.E., ed., *Jet-cloud Interactions in Extragalactic Nuclei*, published on the World Wide Web, <http://www.shef.ac.uk/~phys/research/astro/conf/index.html>
- Barthel, P.D., Miley, G.K., Schilizzi, R.T., Lonsdale, C.J., 1988, *A&AS*, 73, 515
- Baum, S.A., 1992, in Fabian, A.C., ed., *NATO ASI Ser.*, vol. 366, *Clusters and Superclusters of Galaxies*, Kluwer, Dordrecht, p. 171
- Baum, S.A., Heckman, T.M., 1989, *ApJ*, 336, 681
- Bridle, A.H., Perley, R.A., 1984, *ARA&A*, 22, 319
- Bowman, M., Leahy, J.P., Komissarov, S.S., 1996, *MNRAS*, 279, 899
- Burns, J.O., 1986, *Can.J.P.*, 64, 363
- Burns, J.O., O'Dea, C.P., Gregory, S.A., Balonek, T.J., 1986, *ApJ*, 307, 73
- Chambers, K.C., Miley, G.K., van Breugel, W.J.M., 1990, *ApJ*, 363, 21
- Chambers, K.C., Miley, G.K., van Breugel, W.J.M., 1987, *Nat*, 329, 624
- Cowie, L.L., Hu, E.M., Jenkins, E.B., York, D.G., 1983, *ApJ*, 272, 29
- Clark, N.E., Tadhunter, C.N., 1996, in Carilli, C.L., Harris, D.E., eds., *Cygnus A – Study of a Radio Galaxy*, CUP, Cambridge, p. 15
- Crawford, C.S., Vanderriest, C., 1996, *MNRAS*, 285, 580
- De Young, D.S., 1991, *ApJ*, 371, 69
- Dunlop, J.S., 1995, in Hippelein, H., Meisenheimer, K., eds., *Galaxies in the Young Universe*, *Lecture Notes in Physics* vol. 463, Springer-Verlag, Berlin
- Dunlop, J.S., Peacock, J.A., 1993, *MNRAS*, 263, 936
- Fabian, A.C., 1994, *ARA&A*, 32, 277
- Falle, S.A.E.G., 1991, *MNRAS*, 250, 581
- Higgins, S.W., O'Brien, T.J., Dunlop, J.S., 1996, in Ekers, R., Fanti, C., Padrielli, L., *Extragalactic Radio Sources*, IAU Symp. 175, Kluwer, Dordrecht, 467
- Higgins, S.W., O'Brien, T.J., Dunlop, J.S., 1995, in Millar, T.J., Raga, A., eds, *Shocks in Astrophysics*, Kluwer, Dordrecht, p. 311
- Hill, G.J., Lilly, S.J., 1990 *ApJ*, 367, 1
- Icke, V., 1991, in Hughes, P.A., ed, *Beams and Jets in Astrophysics*, CUP, Cambridge, p. 232
- Koide, S., Sakai, J.-I., Nishikawa, K.-I., Mutel, R. L., 1996, *ApJ*, 464, 724
- Lacy, M., Rawlings, S., 1994, *MNRAS*, 270, 431
- Liu, R., Pooley, G., 1991, *MNRAS*, 249, 343
- Leahy, J.P., 1984, *MNRAS*, 208, 323
- Leahy, J.P., Muxlow, T.W.B., Stephens, P.W. 1989, *MNRAS*, 239, 401
- Loken, C., Roettiger, K., Burns, J.O. Norman, M., 1995, *ApJ*, 445, 80L
- Lonsdale, C.J., Barthel, P.D., 1986, *ApJ*, 303, 617
- McCarthy, P.J., 1993, *ARA&A*, 31, 639
- McCarthy, P.J., van Breugel, W., Kapahi, V.K., 1991, *ApJ*, 371, 478
- Meisenheimer, K., Hippelein, H., 1992, *A&A*, 264, 455
- Muxlow, T.W.B, Garrington, S.T., 1991, in Hughes, P.A., ed, *Beams and Jets in Astrophysics*, CUP, Cambridge, p. 51
- Nittman, J., Falle, S.A.E.G. and Gaskell, P.H., 1982, *MNRAS*, 201, 833
- Norman, M.L., 1993, in Burgarella, D., Livio, M., O'Dea, C., eds, *STScI Symp. Ser. Vol. 6, Astrophysical Jets*, CUP, Cambridge, p. 211
- Owen, F.N., O'Dea, C.P., Keel, W.C., 1990, *ApJ*, 352, 44
- O'Donoghue, A.A., Eilek, J.A., Owen, F.N., 1993, *ApJ*, 408, 428
- O'Donoghue, A.A., Owen, F.N., Eilek, J.A., 1990, *ApJS*, 72, 75
- Pedety, J. A., Rudnick, L., McCarthy, P.J., Spinrad, H., 1989, *AJ*, 97, 647
- Pinckney, J., Burns, J.O., Hill, J.M., 1994, *AJ*, 108, 2031
- Raga, A.C., Canto, J., 1996, *MNRAS*, 280, 567
- Rector, T.A., Stocke, J.T., Ellingson, E., 1995, *AJ*, 110, 1492
- Rottgering, H., 1993. *PhD Thesis*, University of Leiden
- Saikia, D.J., Jeyakumar, S., Wiita, P.J., Sanghera, H., Spencer, R.E., 1995, *MNRAS*, 276, 1215
- Sakelliou, I., Merryfield, M.R., McHardy, I.M., 1996, *MNRAS*, 283, 673
- Sanders, R.H., Prendergast, K.H., 1974, *ApJ*, 188, 489
- Scheuer, P.A.G., 1982, in Heeschen, D.S., Wade, C.M., eds, *Extragalactic Radio Sources*, IAU Symp. 97, Reidel, Dordrecht, p. 163
- Smith, M., Norman, M.L., Winkler, K-H.A., Smarr, L., 1985, *MNRAS*, 214, 67
- Sod, Gary A., 1978, *J.Comp.Phys.*, 27, 1
- Steffen, W.S., Gómez, J.L., Raga, A.C. & Williams, R.J.R., 1997, *ApJ*, L73
- Stocke, J.T., Burns, J.O., Christiansen, W.A., 1985, *ApJ*, 299, 799
- Stockton, A., Ridgway, S., Kellog, M., 1996, *AJ*, 112, 902
- Sutherland, R.S., Bicknell, G.V., Dopita, M.A., 1993, *ApJ*, 414, 510
- Tadhunter, C.N., Clark, N., Shaw, M.A., Morganti, R., 1994 *A&A*, 288, L21
- Tadhunter, C.N., 1996, in Carilli, C.L., Harris, D.E., *Cygnus A – Study of a Radio Galaxy*, CUP, Cambridge, p. 33
- van Breugel, W.J.M., Heckman, T.M., George, K., Filippenko, A.V., 1986, *ApJ*, 311, 58
- van Breugel, W.J.M., 1996, in Ekers, R., Fanti, C., Padrielli, L., *Extragalactic Radio Sources*, IAU Symp. 175, Kluwer, Dordrecht, 577
- Williams, A.G., Gull, S.F., 1985, *Nat*, 313, 34
- Wilson, Andrew S., 1993, in Burgarella, D., Livio, M., O'Dea, C., eds, *STScI Symp. Ser. Vol. 6, Astrophysical Jets*, CUP, Cambridge, p. 122
- Wilson, M.J., Scheuer, P.A.G., 1983, *MNRAS*, 205, 449
- Yates, M.G., Miller, L., Peacock, J.A., 1989, *MNRAS*, 240, 129

FIGURE CAPTIONS

Figure 1: The geometry of the computational grid. This shows the symmetry plane containing the jet axis (arrow) and bisecting the cloud (hemisphere). It also shows the view-point used for the density slices in figures 3 to 7, the z -axis.

Figure 2: Example of the results of a test using a one-dimensional problem involving the impact of a shock on a density discontinuity. The solid line represents the analytical solution, the points represent the results of the simulation. The parameter values are: ‘jet’ (shock) Mach number 2.0, pressure 1.0 and density 1.0; ‘cloud’ (discontinuity) pressure 1.0 and density 200.

Figure 3: Logarithmic plots (on the same greyscale) of density in the symmetry plane for the same jet parameters at the same time run at two different resolutions. The upper panel was produced from a simulation run at twice the resolution of the second, then smoothed with a 3-D gaussian and binned down to the same pixel size.

Figure 4: Alternative plots of synchrotron surface brightness distribution, using a logarithmic grey scale. Panels *a*) and *b*) show the effect of changing α on our prescription. Panel *a*) shows the effect of $\alpha = 0.5$, which is the value we use in plots shown elsewhere in this paper. Panel *b*) shows the effect of $\alpha = 1.0$: jet and tail are fainter, so that the wider diffuse emission at the edges of the tail is not seen. Panel *c*) shows pressure squared only where there is jet material. The jet and tail are as bright as in the previous plots, but the diffuse emission around them is not seen due to the negligible magnetic fields in these outer regions, producing a narrower tail. Panel *d*) shows the square of total pressure: this is the effect of allowing the same magnetic field in the ambient medium and the jet.

Figure 5: Logarithmic greyscale plots of total gas density (in the symmetry plane) and integrated radio emission from simulation 1 ($M = 2, \eta_j = 0.01, \eta_c = 50.0$). In the density plots white represents the highest value. For clarity in the radio plots black represents the peak brightness. The plots are shown at two epochs from the simulation: *a*) 56 million years after the jet enters the grid, and *b*) 112 million years.

Figure 6: Logarithmic greyscale plots of total gas density (in the symmetry plane) and integrated radio emission for simulation 4 ($M = 10, \eta = 0.01, \eta_c = 200.0$). In the density plots white represents the highest value. For clarity in the radio plots black represents the peak brightness. The plots are shown at two epochs from the simulation: *a*) 16 million years after the jet enters the grid, and *b*) 56 million years.

Figure 7: Logarithmic greyscale plots of total gas density (in the symmetry plane) and integrated radio emission for simulation 6 ($M = 2, \eta_j = 0.2, \eta_c = 200.0$). In the density plots white represents the highest value. For clarity in the radio plots black represents the peak brightness. The plots are shown at two epochs from the simulation: *a*) 56 million years after the jet enters the grid, and *b*) 112 million years.

Figure 8: Three dimensional velocity vector plots of a Mach 2 jet with density contrast $\eta = 0.2$, seen from two orientations. The jet emerges from the plane of the upper panel. Vectors are plotted if they have a speed greater than 20% of the speed of the incoming jet.

Figure 9: Radio emission seen from two orientations: *(a)* perpendicular to the symmetry plane (as in previous radio

plots), and *(b)* rotated so that the jet axis is about 30° from the line of sight.

Figure 10: Square of density integrated along the line of sight, indicating the expected site of line emission, overlaid with synthesized radio contours corresponding to 9 *a*).

Figure 11: A jet propagating through a collection of clouds. This is a fast, light jet ($M=10, \eta=0.01$). All clouds have density contrast of 50. They are distributed at random positions in the grid, with a fixed volume filling factor of 0.2 and a power law distribution of radius up to a fixed maximum size (1.4 times the radius of the jet). There is no plane of symmetry in this problem, so we had to calculate the whole grid, which in this case was $90 \times 90 \times 90$. This represents a volume of 729000 kpc^3 . The plots show the results about four million years after the jet entered the grid. *a*) A constant density surface of the jet inside a diffuse rendering of cloud density. *b*) A synthetic radio map. The jet has been deflected at least twice, where it has encountered clouds, but clearly remains collimated.

Simulation number	Jet density contrast	Cloud density contrast	Jet mach number	Jet speed
1	0.01	50	2	0.07c
2	0.01	200	2	0.07c
3	0.01	50	10	0.36c
4	0.01	200	10	0.36c
5	0.2	50	2	0.02c
6	0.2	200	2	0.02c
7	0.2	50	10	0.08c
8	0.2	200	10	0.08c
9	0.01	–	2	0.07c
10	0.01	–	2	0.02c
11	0.2	–	10	0.36c
12	0.2	–	10	0.08c

Table 1. The values of the parameters for twelve different simulations. The jet density contrast is the ratio of the jet density to the ambient density; the cloud density contrast is the ratio of the cloud density to the ambient density; the jet mach number is the ratio of the jet speed to the sound speed within the jet. There is no cloud in simulations 9 – 12.

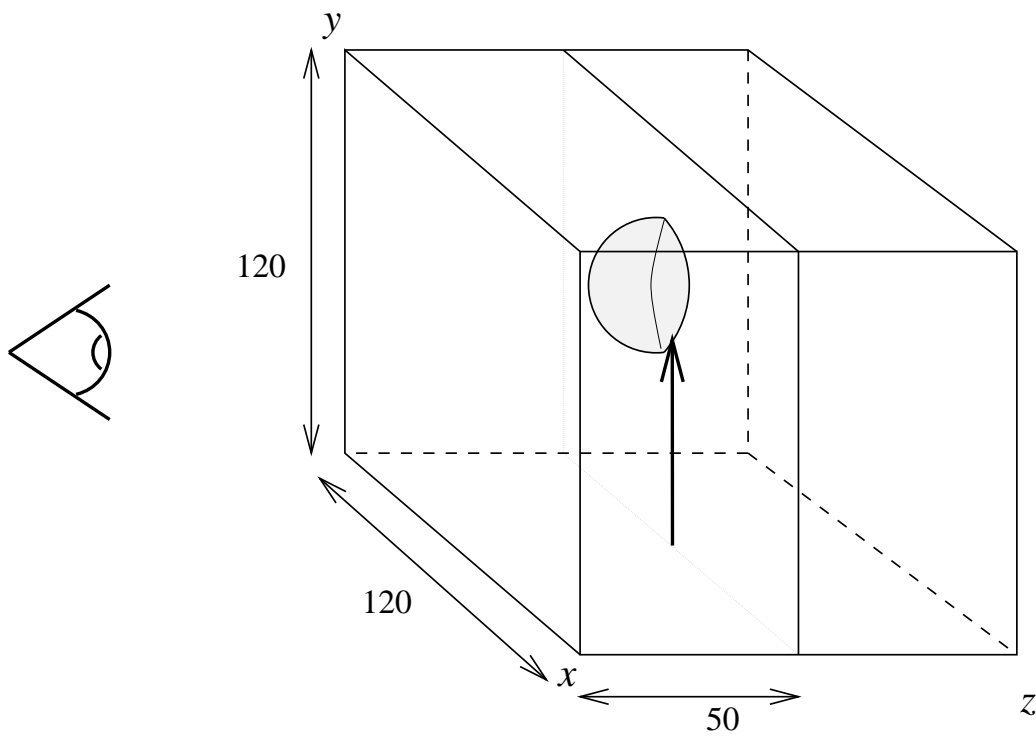


Figure 1.

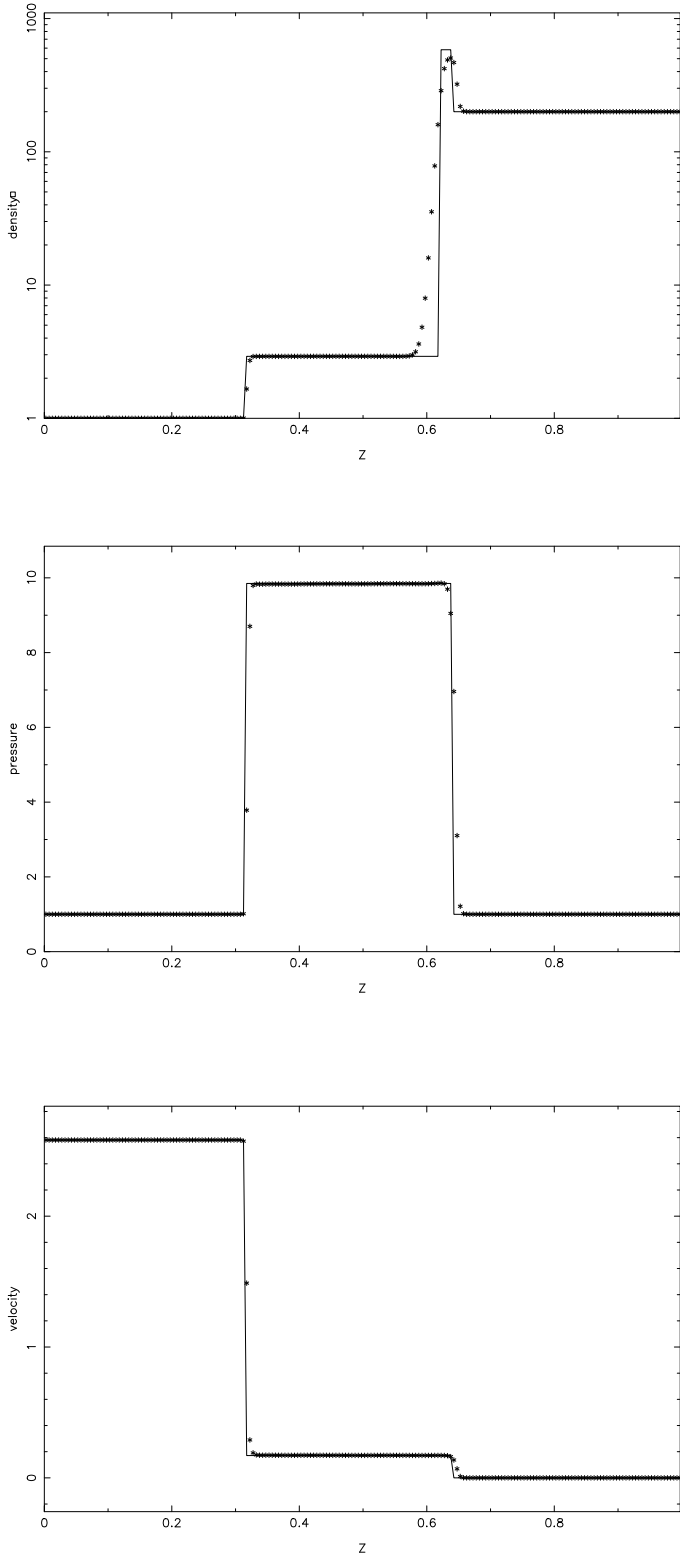


Figure 2.

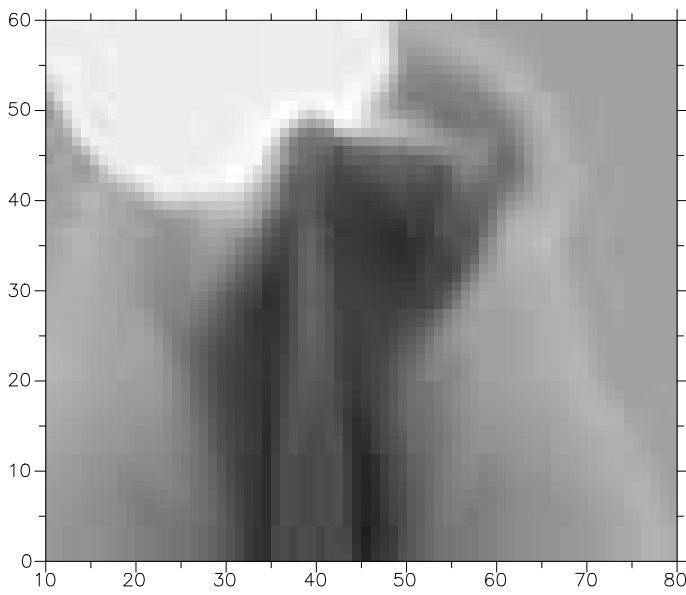
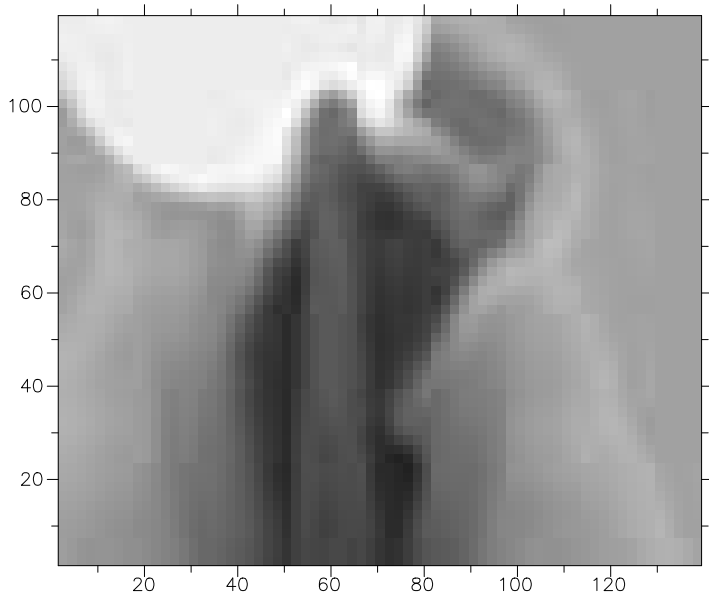


Figure 3.

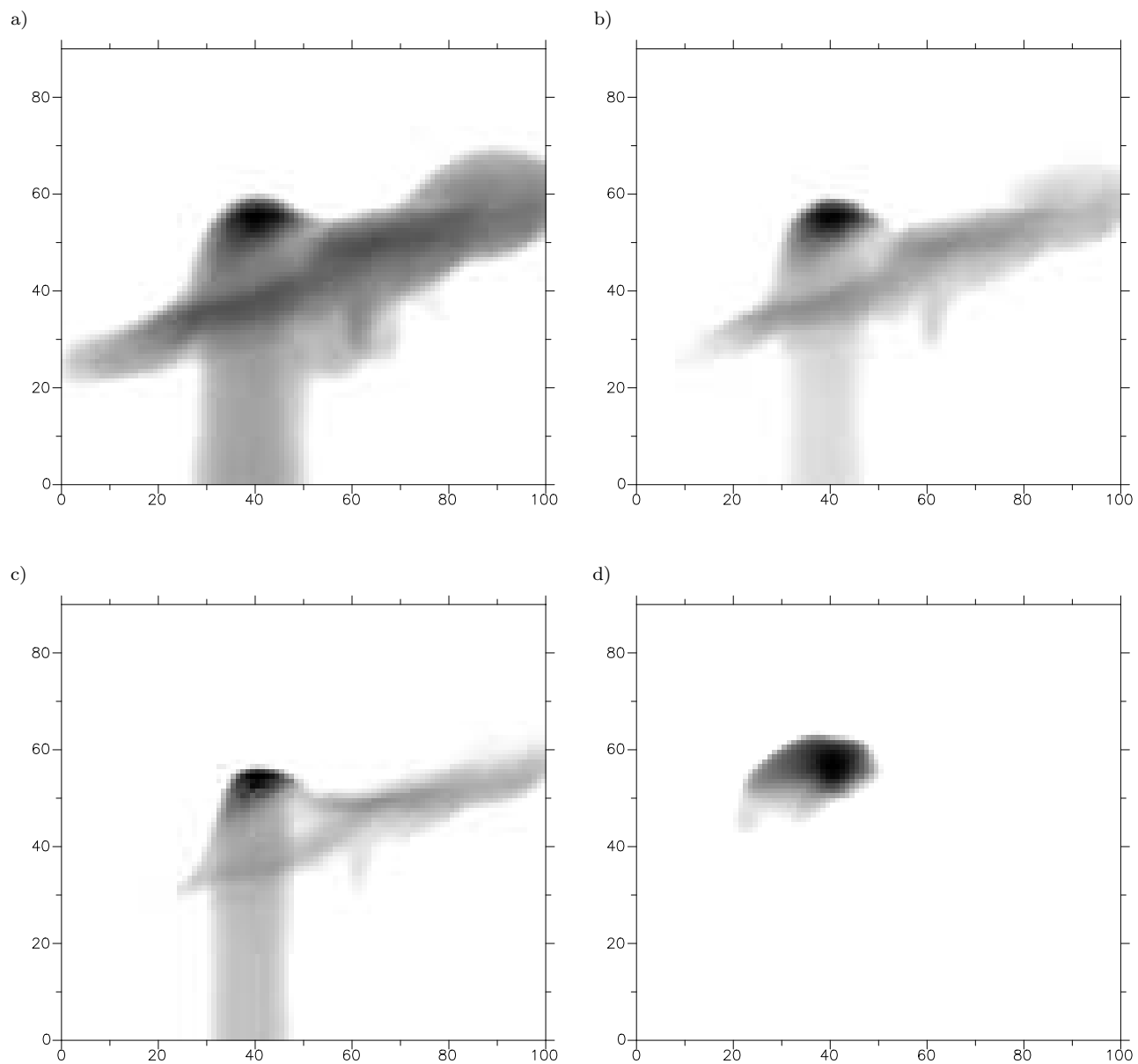


Figure 4.

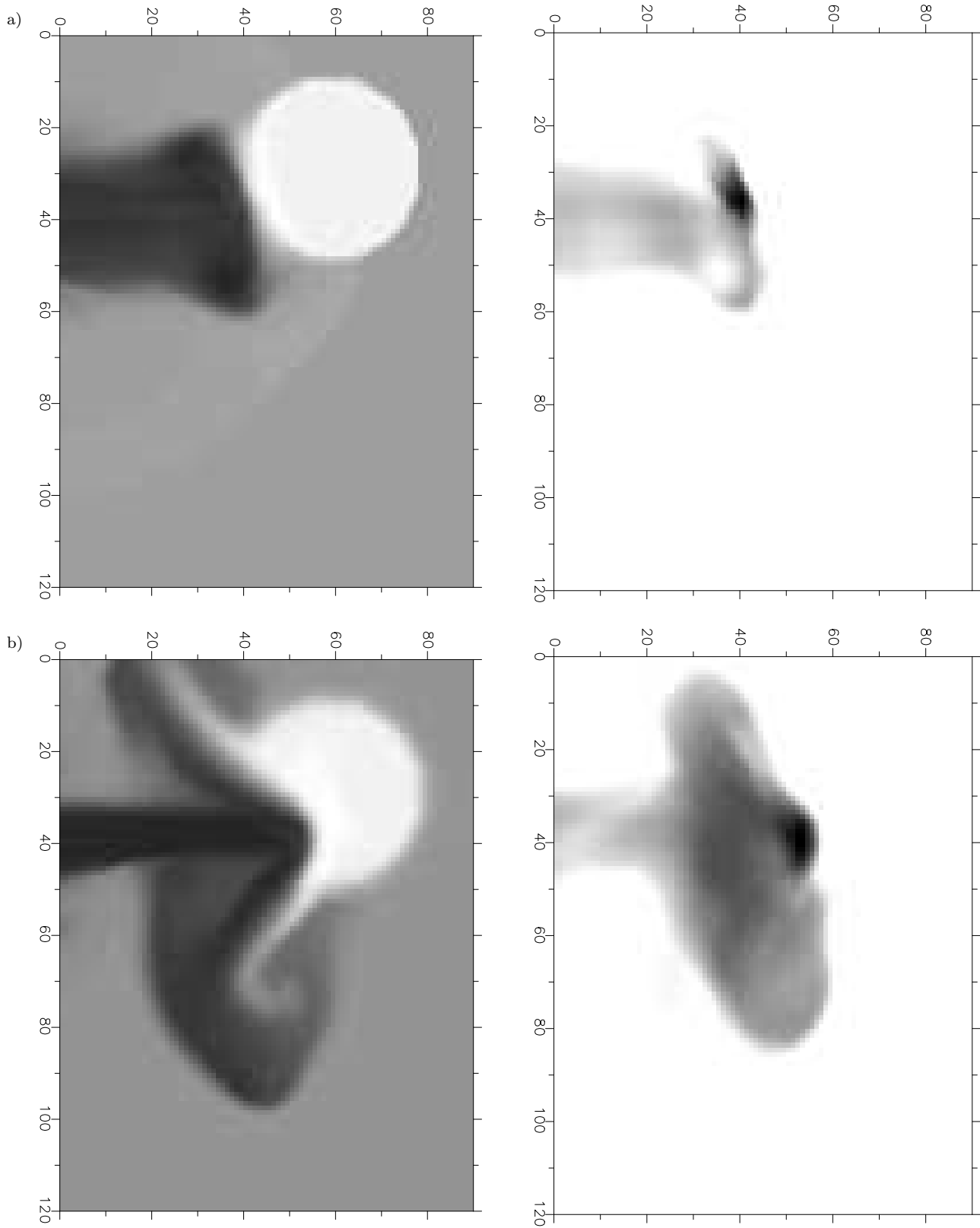


Figure 5.

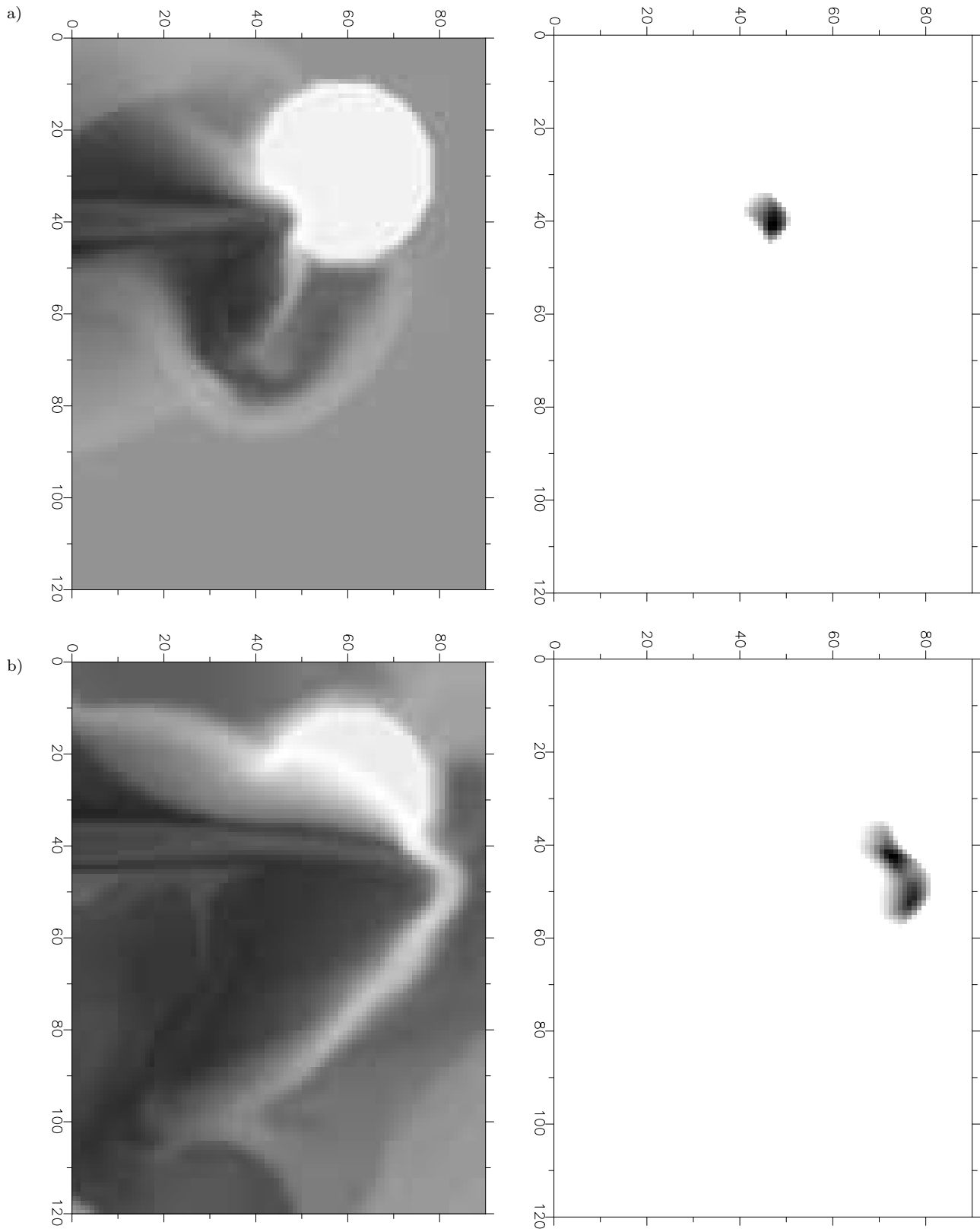


Figure 6.

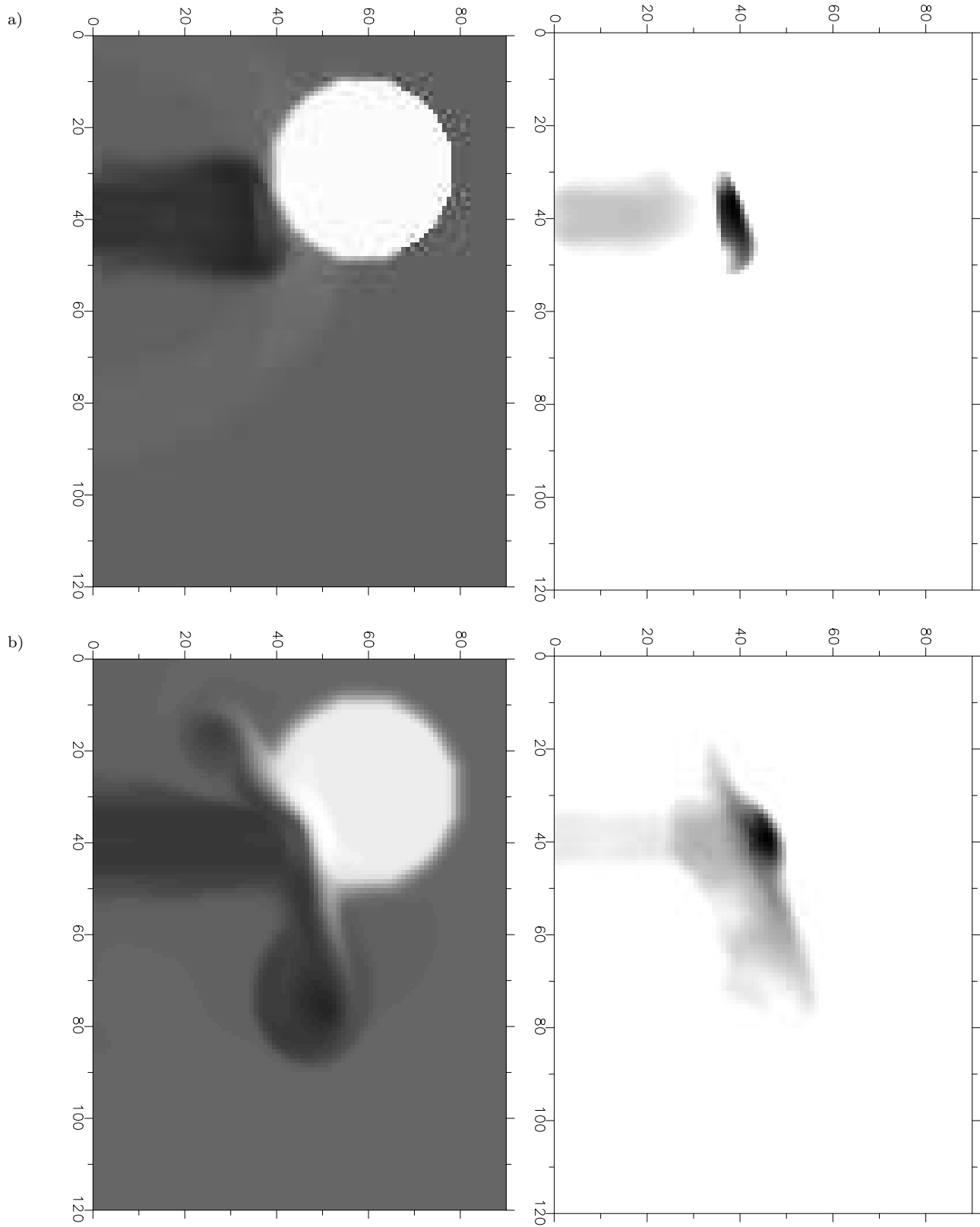


Figure 7.

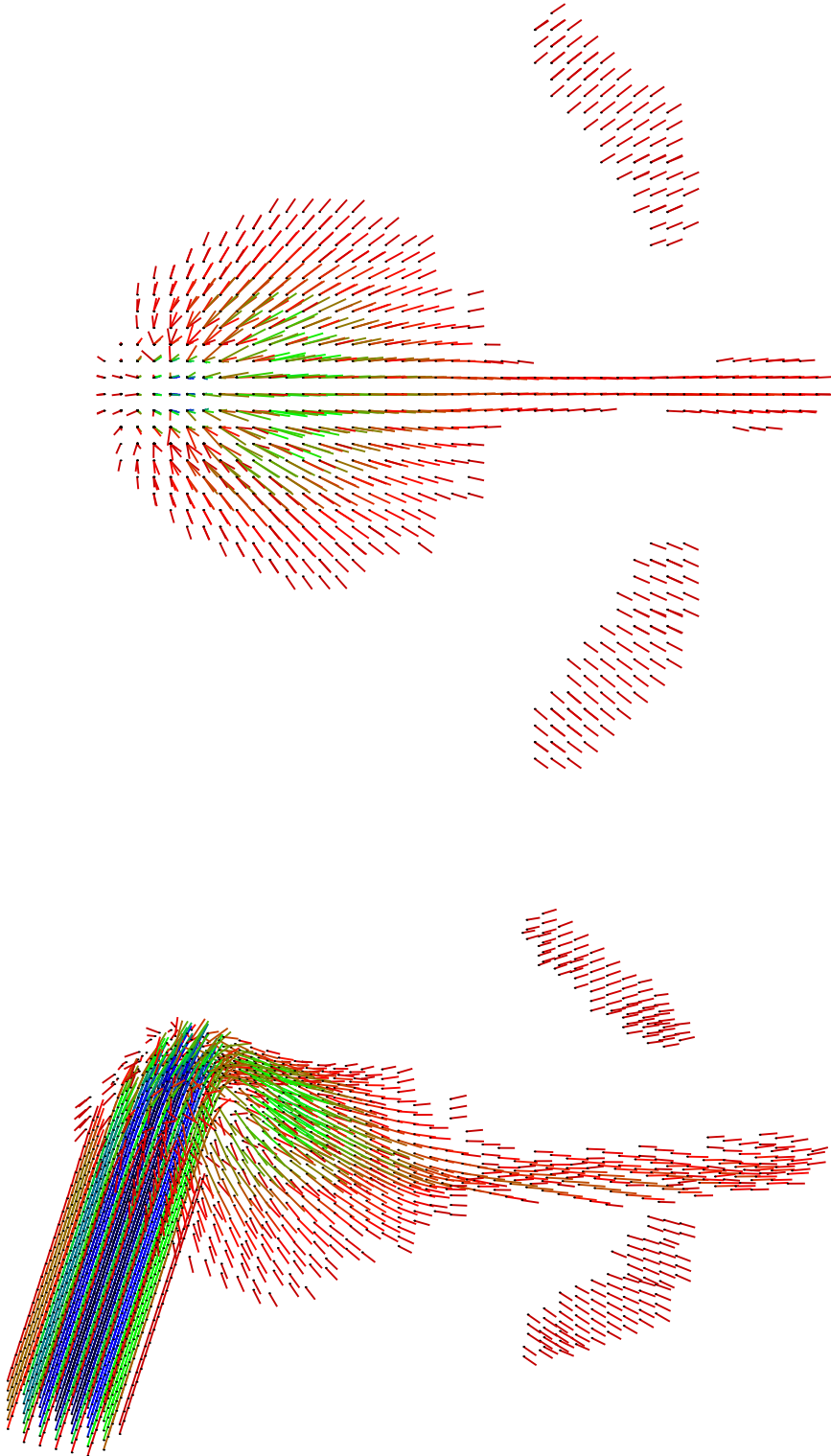


Figure 8.

a)



b)



Figure 9.

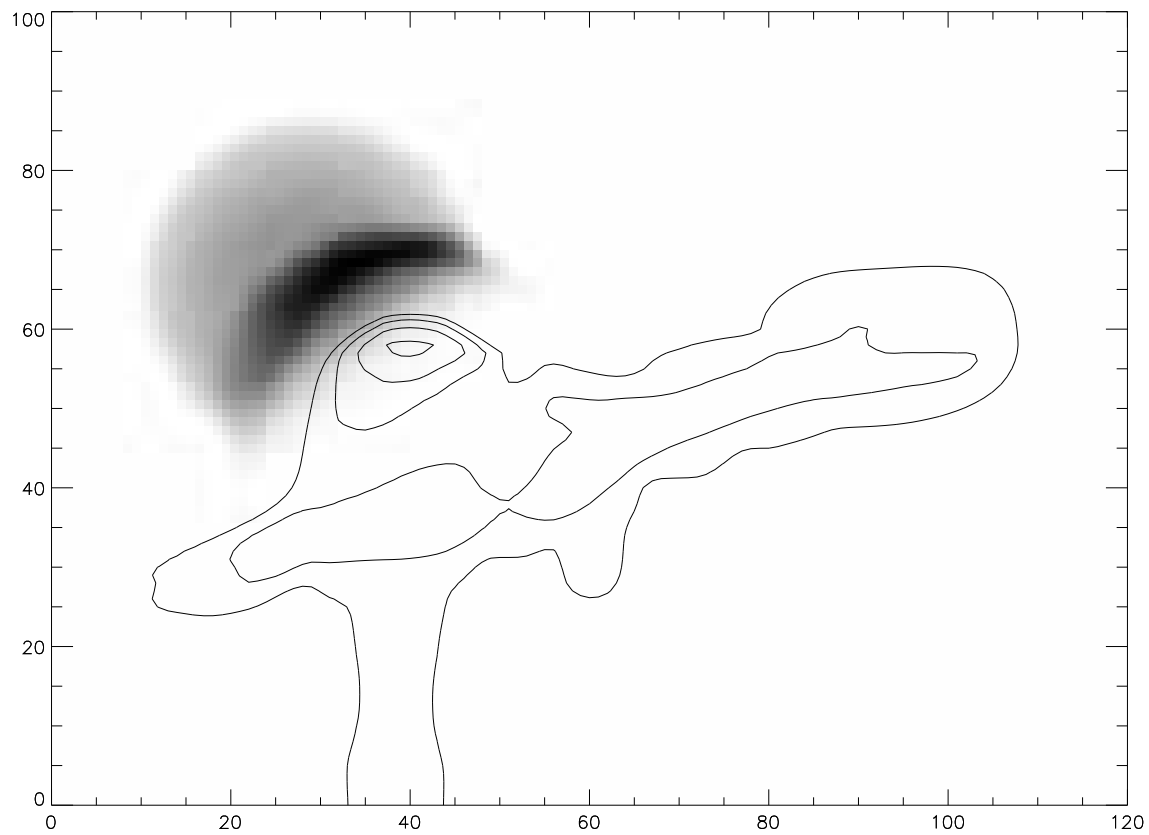
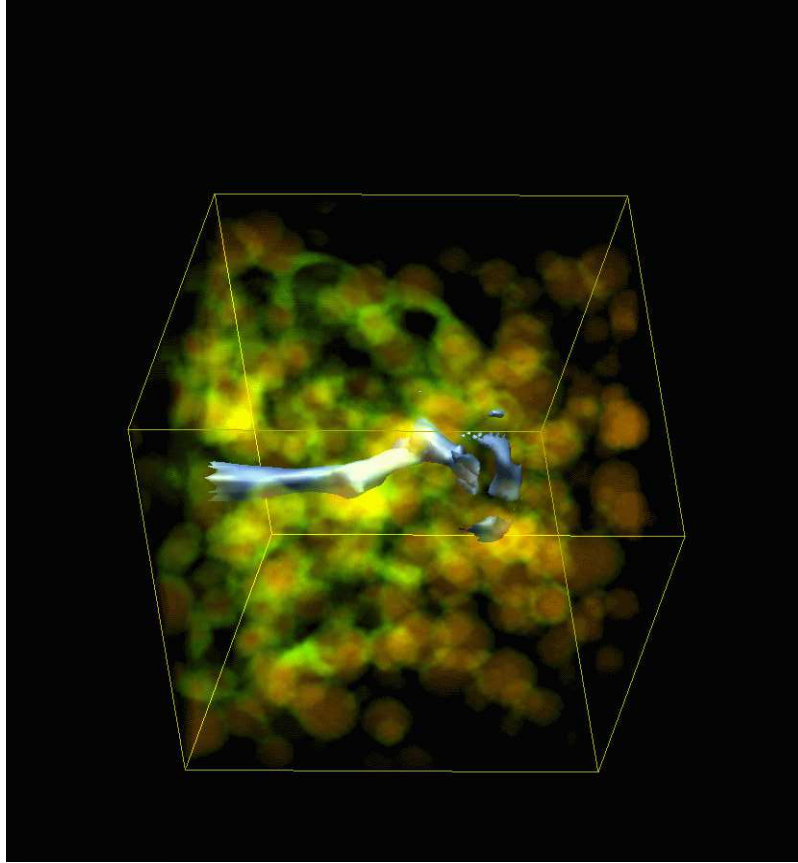


Figure 10.

a)



b)



Figure 11.